Paper published in *Applied Acoustics* 182 (2021) 108270
https://doi.org/10.1016/j.apacoust.2021.108270

A 2.5D acoustic finite element method applied to railway acoustics

Hui Li, David Thompson, Giacomo Squicciarini
Institute of Sound and Vibration Research, University of Southampton,
Southampton SO17 1BJ, United Kingdom

Abstract

Railway acoustic problems commonly have a constant cross-section and uniform properties in the longitudinal direction. To solve such 3D acoustic problems with reduced effort, a wavenumber domain acoustic finite element (2.5D acoustic FE) method is introduced in which the cross-section of the domain is meshed and the third dimension is represented by a wavenumber transform. The acoustic wavenumber is thereby decomposed into a combination of wavenumbers in the x direction and in the y-z plane. The method is extended to exterior noise problems by including a perfectly matched layer (PML) with bespoke absorption to prevent reflection of the sound waves at the boundary of the domain. The method as presented can be used with 2D finite element solutions from commercial software. To verify the application of the 2.5D acoustic FE method for interior acoustic problems, sound attenuation in a tunnel is predicted and compared with existing measurements. To verify the implementation for exterior acoustic problems, an example is given of the sound distribution on the side surface of a train due to a compact source below it. The comparison of the solutions obtained from the 2.5D acoustic FE models with measurements shows good agreement in the both validation cases. The method is then used to investigate the effect of the tunnel walls on the sound distribution on the train external surface by comparing the results with the case in the open field. A highly reverberant sound field is found in tunnels, which increases the sound pressure level on the train side-surface above 250 Hz by about 10 dB for a tunnel with a ballasted track and by about a further 6 dB for a slab track.

Key words: wavenumber domain, 2.5D, finite element method, perfectly matched layer, railway acoustics.

1. Introduction

The noise inside trains can affect the comfort of passengers and train crew. Zhang et al. [1] measured the noise levels inside 134 trains of similar design when they were running at about 300 km/h. They found that inside 87% of these trains, the sound pressure levels (SPL) ranged from 72-79 dB(A) at the ends of the passenger compartment and were about 3-5 dB(A) lower in the middle of the carriages. Moreover, noise levels inside train cabins will be higher if they run in tunnels [2, 3]. Measurements have shown that the interior noise of a German inter-city train increased by about 10 dB(A) when it was running in a tunnel with a ballasted track at 250 km/h, while if the tunnel had ballastless track, the interior noise level increased by a further 7 dB(A) [2]. Choi et al. [3] measured the noise inside Korean high-speed trains when they were running in tunnels with slab or ballasted track. Compared with the situation in the open field or on a viaduct, the interior noise levels in tunnels with ballasted tracks were approximately 10 dB(A) higher and the values in tunnels with slab tracks were 15 dB(A) higher. Although the speeds of metro railway vehicles are generally much lower than those of inter-city trains, the interior noise in metro railway vehicles is not necessarily lower than in mainline trains because of insufficient sealing of the metro cars (metro vehicles have more doors than trains) and the enclosed environment of the tunnels [4]. The noise induced by railway vehicles will also cause impact to the surrounding environment. Because of the high levels of noise caused by railway vehicles, noise barriers [5] are commonly used to prevent the influence to the surrounding environment.

Given the range of acoustic problems associated with railways [6], efficient prediction methods are required. Prediction of both interior and exterior noise caused by railway vehicles can be a challenging task, especially in the middle-high frequency range, as railway vehicles have large dimensions. Generally, solutions for acoustic problems can be obtained by numerical methods, such as the finite element (FE) or boundary element (BE) methods [7] but unfortunately, the requirement to include at least six elements per wavelength becomes very demanding at high frequencies, especially for spaces that are extended in one or more dimensions. Therefore, simulations by FE/BE methods are only feasible for cases with limited dimensions and at low frequencies. Alternative approaches have been used for acoustic problems associated with railway vehicles with varying success. For instance, the statistical energy analysis (SEA) method [8] has a reputation for solving problems associated with large structures, with small computational effort. The SEA method has been used to investigate the noise inside train cabins

[9, 10]. Forssén et al. [9] employed an SEA model to predict the noise inside a 1:5 scale railway vehicle for the whole frequency range of interest. Sadri et al. [10] used an SEA model to predict the noise inside a full scale passenger vehicle. The predicted SPLs in the train cabin along its longitudinal direction were in reasonable agreement with the measured results at most frequencies. However, even though the SEA approach has shown its advantages for predicting the interior noise, the conventional SEA requires subsystems to be 'weakly coupled' [11] which is not always satisfied. Besides, SEA models require there to be sufficient modes in each subsystem within each frequency band to ensure a diffuse field [11]. Some problems have been found in using the SEA approach to model acoustic environments in a long space [12], which is the case for noise inside train cabins or inside tunnels.

The ray tracing method can be used to predict the noise around and inside a railway vehicle [13]. This is based on a high frequency assumption which treats the sound waves like ray trajectories [14]. In the ray tracing method, the amplitude of the acoustic pressure varies along the wave fronts depending on the density of the ray trajectories [14]. The early applications of the ray tracing method can be dated back to the 1940s when Blokhintzev [15] studied the sound propagation in an inhomogeneous and moving medium. In railway applications, Bistagnino et al. [16] adopted a beam-tracing technique to predict the SPL on the external walls of a train due to rolling noise. Kohrs et al. [13] used a ray tracing model to simulate the sound field around a metro vehicle in a tunnel and another ray tracing model to predict the sound field around the metro vehicle in the open field.

Li et al. [17] developed a numerical model based on an image source method to study the noise attenuation in full scale road traffic tunnels and found good agreement with measurements. In their model, the total sound pressure at a receiver was computed by summing contributions from all image sources coherently. They also allowed for the atmospheric absorption of sound in air. Using a similar method, Fung [18] predicted the sound propagation in a railway tunnel. In practice, the image source method requires an appropriate number of image sources to achieve converged predictions. With this approach, if the shape of the tunnel cross-section is arbitrary, the reflections and the image source locations are difficult to determine.

A common feature of many problems associated with railway noise is that the geometry is effectively uniform in one direction. Considering the computational difficulty of using a 3D FE/BE method to predict the noise caused by large objects, some authors have used 2D models

to achieve higher efficiency [19, 20]. For example, Hothersall et al. [19] presented numerical results for 2D diffraction problems to study the insertion loss of a noise barrier. Zhang et al. [20] investigated the sound radiation of the railway track including the proximity of the ground by using the BE method in 2D. However, the 2D models cannot fully take into account the corresponding 3D effects. For instance, Zhang et al. [20] found that some corrections were necessary at low frequency in terms of the radiation efficiency of the track.

Taking advantage of the 2D nature of the geometry, some researchers have used a 2.5D BE method to solve 3D acoustic problems for such situations [5, 21]. In the 2.5D BE method, only the cross-section of the problem is represented by using boundary elements, while the variations in the third direction are considered in terms of a spectrum of wavenumbers. An inverse Fourier transform is applied to obtain the sound pressure in the spatial domain. One of the first applications of the 2.5D BE method in acoustics was made by Duhamel [5] to predict the sound pressure around a noise barrier with constant properties in one direction but with arbitrary cross-section. The method showed high efficiency and accuracy for such a problem. Li et al. [21] utilised the 2.5D BE method to predict the propagation of rolling noise to the train external surfaces. The vibrating surface of the rail was treated directly as a source in the wavenumber domain and a method of representing point sources in the 2.5D approach was developed to represent the wheel.

For such problems that have uniform properties in one direction, a BE method based on periodic structures can also be used to reduce the computational effort. This type of method is based on the assumption that the surface pressure on the periodic structure at two periodic points is related by a constant factor $e^{\gamma L}$, where L is the chosen length of a representative segment of the periodic structure and γ is generally a complex value. Using this method, the original acoustic problem is reduced to the modelling of just one period of the structure. Lam [22] developed this periodic BE method and used it for the prediction of acoustic scattering from periodic structures due to plane waves and point sources in the near field of a surface. This approach, which has been referred to as quasi-periodic BEM, has been developed further by Fard et al. [23] and Ziegelwanger [24] et al.. It requires the geometry, boundary conditions and sound pressure field along the longitudinal axis direction to be periodic. Karimi et al. [25] developed a block Toeplitz matrix formulation for 3D acoustic scattering problems from periodic structures which requires periodicity of geometry but allows an arbitrary sound field. They applied it to two acoustic problems associated with continuous and discrete structures to

verify their method. Their results have showed good accuracy and reduced computational time and storage requirements. Similar approaches based on periodic structure theory have been used in structural FE [26] but the authors are not aware of application to acoustic FE.

The FE method has some advantages over the BE method, especially for enclosed domains. Nilsson and Finnveden [27] developed a 2.5D fluid-solid coupled FE method to study the structural wave propagation in thin-walled fluid-filled ducts with arbitrary cross-section. Their 2.5D fluid FE model can solve for the sound pressure induced by structural vibration but it has to be coupled with FE or BE models to provide the excitation. Because their 2.5D fluid FE method was formed in a solid FE sense, acoustic boundary conditions, such as acoustic impedance and imposed normal velocity, cannot be easily included.

For exterior noise problems, the BE method directly allows for the Sommerfeld far field radiation condition, whereas with the FE method reflections can occur at the domain boundaries. Nevertheless, to allow coupling with an unbounded surrounding medium, a perfectly matched layer (PML) [28] can be used in the FE method. For instance, Zuo and Fan [29] used a 2.5D FE method (also called a semi-analytical FE, or SAFE, method) with a PML for a modal study of waveguides with arbitrary cross-sections immersed in fluid. For pipe-like structures, the two dimensional SAFE-PML approach can even be reduced to a one-dimensional problem by rearranging the problem in cylindrical coordinates [30]. Song et al. [31] combined a 2.5D infinite element model with a modal acoustic transfer vector method to study noise from railway bridges. The 2D cross-section of the bridge was created to calculate an acoustic transfer vector from a source to a receiver and a spatial inverse Fourier transform was then applied to obtain the 3D acoustic transfer vector. The dynamic response of the bridge was calculated in a 3D model and used in combination with the acoustic transfer vector to obtain the bridge noise.

Based on the above, the aim of this paper is to implement a wavenumber domain acoustic finite element (2.5D acoustic FE) method and apply it to various acoustic problems associated with railway vehicles and tunnels. Different from these previous 2.5D FE models, this paper presents a derivation of the 2.5D acoustic FE method from the classical wave equation, which can allow the inclusion of acoustic boundary conditions and internal noise sources. It is complementary to the 2.5D BE method [21], and allows internal sources to be included more conveniently and there is no need to deal with the non-uniqueness problems. It also avoids the

non-uniqueness problem inherent in the BE method. Moreover, the method as presented can directly make use of 2D solutions obtained from commercial software. Section 2 presents the derivation of the 2.5D acoustic FE method from the Helmholtz equation and its extension to a free field by applying a PML [28]. Section 3 presents two validation cases for the use of this method in calculating railway noise in tunnels and in open field. Section 4 investigates the effect of the tunnel on the sound distribution on the train external surface, which constitutes a combination of the two validation cases. A short discussion of the method is given in Section 5 and the conclusions in Section 6.

2. 2.5D acoustic finite element model

The numerical procedure of the 2.5D acoustic FE method is presented in this Section, allowing acoustic problems to be solved in a situation with uniform properties and geometry in one direction by using a 2D geometry. The starting point for the formulation is a weak form of the Helmholtz equation [32] written in the wavenumber domain (2.5D) for ducts of arbitrary cross-section.

2.1. The weak form of the Helmholtz equation in the 2.5D domain

The homogeneous Helmholtz equation for time-harmonic linear acoustic problems is

$$\nabla^2 p + k^2 p = 0 \tag{1}$$

where p is the acoustic pressure amplitude and $k = \omega/c_0$ is the wavenumber, with ω the circular frequency and c_0 the wave speed (343 m/s). It is first assumed that the acoustic domain is bounded and has constant geometry and properties in the x direction, as shown in Figure 1. The sound pressure field can be written in terms of a Fourier transform pair over x:

$$p(x,y,z) = \frac{1}{2\pi}\int_{-\infty}^{\infty} \tilde{p}(k_x,y,z)\, \mathrm{e}^{-\mathrm{i}k_x x}\mathrm{d}k_x \tag{2}$$

$$\tilde{p}(k_x, y, z) = \int_{-\infty}^{\infty} p(x, y, z)\, \mathrm{e}^{\mathrm{i}k_x x} \mathrm{d}x \tag{3}$$

Substituting this into Eq. (1), yields

$$\nabla_\perp{}^2 \tilde{p} + (k^2 - k_x^2)\tilde{p} = 0 \tag{4}$$

where the tilde is used to identify quantities in the wavenumber domain. $\nabla_\perp$ is the gradient operator in the *y*-*z* plane which has the form:

$$\nabla_\perp{}^2 = \frac{\partial^2}{\partial y^2} + \frac{\partial^2}{\partial z^2} \tag{5}$$

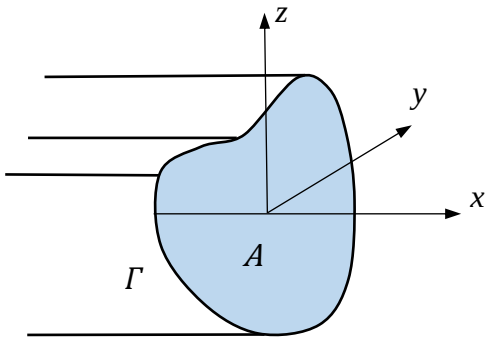

Figure 1. Acoustic domain in a duct of arbitrary cross-section with uniform properties in the *x* direction. *A* is the cross-section area and *Γ* is the cross-section perimeter.

As Eq. (4) is valid anywhere in the acoustic domain, a weak statement [32] for Eq. (4) is

$$\int_V W\left[\nabla_\perp{}^2 \tilde{p} + (k^2 - k_x^2)\tilde{p}\right] \mathrm{d}V = 0 \tag{6}$$

where *W* is an arbitrary continuous function that is defined in the whole acoustic domain *V*. It can be seen that if Eq. (4) is guaranteed within the whole acoustic domain, Eq. (6) will be guaranteed. It is more difficult to prove it rigorously the other way around, hence it is called the 'weak form', but it is reasonable to assume Eq. (4) and Eq. (6) are equivalent [32]. By using the following identity:

$$W\ \nabla_\perp{}^2\tilde{p} = \nabla_\perp \cdot (W\ \nabla_\perp\tilde{p}) - \nabla_\perp W\ \cdot \nabla_\perp\tilde{p} \tag{7}$$

Eq. (6) can be rearranged as

$$\int_x \left(\int_A \{[\ \nabla_\perp \cdot (W\ \nabla_\perp\tilde{p})] + [\ -\nabla_\perp W \cdot \nabla_\perp\tilde{p} + (k^2 - k_x^2)W\tilde{p}]\}\, \mathrm{d}y\mathrm{d}z \right) \mathrm{d}x = 0 \tag{8}$$

where A is the area of the duct cross-section. Because Eq. (8) is valid for any continuous function W, and besides, the pressure $\tilde{p}$ at a given wavenumber k_x is independent of x, this yields the weak form of the Helmholtz equation in 2.5D, after applying the divergence theorem [33], as

$$\int_\Gamma (W\ \nabla_\perp\tilde{p}) \cdot \mathbf{n}\, \mathrm{d}\Gamma + \int_A [\ -\nabla_\perp W \cdot \nabla_\perp\tilde{p} + (k^2 - k_x^2)W\tilde{p}]\, \mathrm{d}y\mathrm{d}z = 0 \tag{9}$$

where Γ is the perimeter of the cross-section and **n** is the normal vector outward from the fluid.

2.2 Boundary conditions in the 2.5D domain

The first term involving $\nabla_\perp\tilde{p}$ in Eq. (9) can be implemented as a boundary condition. It can be derived from the momentum conservation equation in the corresponding 3D domain. In 3D, the momentum conservation equation is expressed as:

$$\rho_0 \frac{\mathrm{d}\mathbf{v}}{\mathrm{d}t} + \nabla p = 0 \tag{10}$$

where ρ_0 is the density of air, 1.21 kg/m^3. **v** is the particle velocity, which can be written using a Fourier transform pair similar to Eq. (2, 3). In the wavenumber domain, therefore, $\nabla_\perp\tilde{p}$ is then expressed in terms of $\tilde{\mathbf{v}}$ as:

$$\nabla_\perp\tilde{p} = -\mathrm{i}\omega\rho_0\tilde{\mathbf{v}} \tag{11}$$

Eq. (11) is a velocity boundary condition in the 2.5D domain. An impedance boundary condition can be applied similarly by using $p/(\mathbf{v} \cdot \mathbf{n}) = Z$, with Z the acoustic impedance and

$\mathbf{v} \cdot \mathbf{n}$ the velocity normal to the surface. The acoustic impedance boundary condition in the 2.5D domain is therefore expressed as:

$$\nabla_{\perp}\tilde{p} \cdot \mathbf{n} = -\mathrm{i}\omega\rho_0 \frac{\tilde{p}}{Z} \tag{12}$$

2.3 2.5D acoustic FE model in matrix form

In the FE sense, the domain can be discretised into elements. The pressure can be approximated by interpolation of the pressure at the element nodes, expressed as:

$$\tilde{p}(k_x, y, z) = \sum_{i=1}^{n} N_i(y, z)^{\mathrm{T}} \tilde{p}_i(k_x) \tag{13}$$

where $\mathbf{N} = [N_1, N_2, \cdots\ N_i]^{\mathrm{T}}$ is the shape function in the *y*-*z* plane and $\tilde{\boldsymbol{p}} = [\tilde{p}_1, \tilde{p}_2, \cdots\ \tilde{p}_i]^{\mathrm{T}}$ is the nodal pressure vector in the wavenumber domain; $^{\mathrm{T}}$ indicates the transpose. Because W can be any continuous function, here it is set as the FE shape function in the *y*-*z* plane, $W = N_i(y, z)$. Then each term in Eq. (9) can be rearranged as:

$$\begin{gathered}
\int_A [\,-\nabla_{\perp} W\ \cdot \nabla_{\perp}\tilde{p}]\,\mathrm{d}y\mathrm{d}z = \int_A -\left[\frac{\partial \mathbf{N}}{\partial y}\frac{\partial \mathbf{N}^{\mathrm{T}}}{\partial y} + \frac{\partial \mathbf{N}}{\partial z}\frac{\partial \mathbf{N}^{\mathrm{T}}}{\partial z}\right]\tilde{\boldsymbol{p}}\,\mathrm{d}y\mathrm{d}z \\
\int_A [-k_x^2 W\tilde{p}]\,\mathrm{d}y\mathrm{d}z = (-\mathrm{i}k_x)^2 \int_A [\mathbf{N}\mathbf{N}^{\mathrm{T}}]\tilde{\boldsymbol{p}}\,\mathrm{d}y\mathrm{d}z \\
\int_A [k^2 W\tilde{p}]\,\mathrm{d}y\mathrm{d}z = \frac{\omega^2}{c_0^2}\int_A [\mathbf{N}\mathbf{N}^{\mathrm{T}}]\tilde{\boldsymbol{p}}\,\mathrm{d}y\mathrm{d}z \\
\int_{\Gamma} (W\,\nabla_{\perp}\tilde{p}) \cdot \mathbf{n}\,\mathrm{d}\Gamma = -\mathrm{i}\omega\rho_0 \int_{\Gamma} \frac{1}{Z}\,[\mathbf{N}\mathbf{N}^{\mathrm{T}}]\tilde{\boldsymbol{p}}\mathrm{d}\Gamma - \mathrm{i}\omega\rho_0 \int_{\Gamma} \mathbf{N}\,\tilde{\mathbf{v}} \cdot \mathbf{n}\mathrm{d}\Gamma
\end{gathered} \tag{14}$$

Eventually, Eq. (9) can be written in matrix form as:

$$[(-\mathbf{K_{11}}(-\mathrm{i}k_x)^2 + \mathbf{K_{00}} - \omega^2\mathbf{M}) + \mathrm{i}\omega\mathbf{C}]\,\tilde{\boldsymbol{p}} = \mathbf{F} \tag{15}$$

where

$$\mathbf{K_{11}} = \int_A [\mathbf{N}\mathbf{N}^{\mathrm{T}}]\,\mathrm{d}y\mathrm{d}z$$

$$\mathbf{K_{00}} = \int_A \left[\frac{\partial \mathbf{N}}{\partial y}\frac{\partial \mathbf{N}^{\mathrm{T}}}{\partial y} + \frac{\partial \mathbf{N}}{\partial z}\frac{\partial \mathbf{N}^{\mathrm{T}}}{\partial z}\right]\mathrm{d}y\mathrm{d}z$$

$$\mathbf{M} = \frac{1}{c_0^2}\int_A [\mathbf{N}\mathbf{N}^{\mathrm{T}}]\,\mathrm{d}y\mathrm{d}z \tag{16}$$

$$\mathbf{C} = \frac{\rho_0}{Z}\int_\Gamma [\mathbf{N}\mathbf{N}^{\mathrm{T}}]\mathrm{d}\Gamma$$

$$\mathbf{F} = -\mathrm{i}\omega\rho_0 \int_\Gamma \mathbf{N}\,\tilde{\mathbf{v}}\cdot\mathbf{n}\mathrm{d}\Gamma$$

The matrix **C** comes from the acoustic impedance conditions and **F** contains the velocity boundary conditions. $\mathbf{K_{00}}$ and $\mathbf{K_{11}}$ are equivalent to stiffness matrices and **M** is equivalent to a mass matrix.

An internal source can be expressed by the Fourier transform of the source strength $\tilde{Q}(k_x, y, z)$, in which the strength distribution in the *x* direction is considered as a spectrum of wavenumber k_x. Analogously to Eq. (9), the internal source term will be expressed as:

$$\mathbf{F}^{\mathrm{q}} = \int_A \mathbf{N}\,\tilde{Q}(k_x, y, z)\,\mathrm{d}y\mathrm{d}z \tag{17}$$

If the internal source is a compact source located at the i^{th} node at (x_0, y_0, z_0), which has the form $Q\delta(x - x_0)\delta(y - y_0)\delta(z - z_0)$, where $Q = \mathrm{i}\omega\rho q_0$ and $q_0$is the volume velocity, after applying the Fourier transform to convert it to the wavenumber domain, the strength distribution is independent of wavenumber k_x. The force vector caused by the internal source term will be added to the vector **F** in Eq. (15).

Eq. (15) can be solved for each frequency and wavenumber. After the sound pressure is determined as a function of wavenumber k_x, the sound pressure in the spatial domain can be obtained from Eq. (2).

2.4 Extension of the method to exterior acoustic problems

In general, far from any sources, the solution of Eq. (1) consists of outgoing sound waves with the form [29]:

$$p(r) = \frac{A}{4\pi r}\,\mathrm{e}^{-\mathrm{i}kr} \tag{18}$$

The acoustic wavenumber is real, indicating the propagation of sound waves to the far field at a *r* distance away from the source and Eq. (18) also shows that in the process the amplitude of the sound, *A*, reduces as 1/*r*. If an imaginary part is added to the wavenumber,

$$p(r) = \frac{\mathrm{A}}{4\pi r}\,\mathrm{e}^{-\mathrm{i}(k-\mathrm{i}\sigma_r)r} = \frac{\mathrm{A}}{4\pi r}\,\mathrm{e}^{-\mathrm{i}k(1-\frac{\mathrm{i}\sigma_r}{k})r} \tag{19}$$

This introduces additional attenuation to the sound pressure when it propagates outwards. This can be achieved in an FE model by including a perfectly matched layer (PML) [28] outside the acoustic domain. Clearly, an infinitely thick PML (*r* infinite) produces no reflection and sound waves are attenuated exponentially as *r* increases. However, to obtain a practical method the PML must be truncated at a finite thickness, say, *D*. Generally, the parameter σ_r, which is called an 'absorption coefficient' in ref. [28], is varied gradually in the PML domain. To achieve a continuous boundary at the interface between the acoustic domain and the PML, σ_r is arranged to increase within the PML from zero at the interface to σ_m at the outer boundary of the PML. This absorption coefficient of the PML is written as [28]

$$\sigma_r(l) = \sigma_m \left(\frac{l}{D}\right)^n \tag{20}$$

where *D* is the thickness of the PML domain and *l* is the distance from the interface into the PML. The reflection at the outer boundary of the PML is estimated as [28]

$$\exp \int_0^D -\sigma_m \left(\frac{l}{D}\right)^n \mathrm{d}l = \mathrm{e}^{-\sigma_m D/(n+1)} \tag{21}$$

The parameters of the PML can thus be adjusted for the desired absorption. Experience suggests [28] that a value of $\sigma_m D/(n+1) = 8$ would give satisfactory results.

When the PML is applied in the 2.5D acoustic FE model, it is the transverse wavenumber in the *y*-*z* plane that needs to be modified within the PML. This is performed by replacing the transverse wavenumber in Eq. (9) by

$$k_{yz}\left(1-\frac{\mathrm{i}\sigma_r}{k_{yz}}\right) \tag{22}$$

where $k_{yz}=(k^2-k_x^2)^{1/2}$ is the wavenumber in the *y*-*z* plane. Since the *x* direction in the 2.5D method is assumed to be infinite, there is no need to apply any attenuation in that direction.

2.5 Implementation

The types of FE used in conventional 2D acoustic analysis can be utilised in a straightforward manner in the 2.5D sense. The system matrices $\mathbf{K_{00}}$, **M**, **C** included in Eq. (15) are the equivalent stiffness, mass, damping matrices in usual 2D acoustic FE models with *k* replaced by k_{yz}. **F** is equivalent to an external force vector. The matrix $\mathbf{K_{11}}$ has similar form to the mass matrix **M** and can be obtained by multiplying **M** with c_0^2. For situations with large dimensions and at high frequencies, there are benefits to employ commercial software to generate these matrices. In the applications in Sections 3 and 4 in this paper, COMSOL is employed to obtain the system matrices. The PML can also be added in the COMSOL model before the system matrices are created. The analysis is performed by using a bespoke PML following the above procedure.

3. Validation cases

Two validation cases are considered in this Section. The first concerns the attenuation of sound in a tunnel and the second the distribution of sound on the exterior of a vehicle in free field.

3.1. Application to interior acoustic problems: sound attenuation in a tunnel

The 2.5D acoustic FE method can be effective and efficient to predict noise in tunnels. A measurement of sound attenuation carried out inside a circular metro tunnel in Sheung Wan station, Hong Kong [18] is employed here to verify the 2.5D acoustic FE model for prediction of noise in tunnels. The geometry of the tunnel in the measurement [18] is shown in Figure 2. It had a cross-section area of approximately 21 m^2, a radius of 2.7 m and the floor had a width

of 2.9 m. The height of the tunnel from the floor is 4.7 m. The tunnel wall in the measurement was of spheroidal graphite iron with segmental embedded concrete lining finish and its floor was cast-in hard concrete laid with rails.

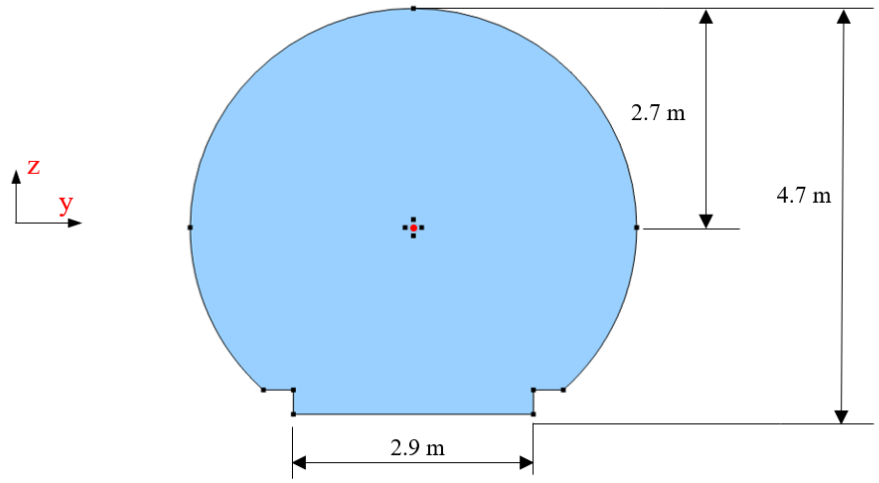

Figure 2. Geometry of the railway tunnel in the measurement, redrawn from [18]. The red circle (•): source; black squares (■): receivers.

The acoustic absorption coefficient of the tunnel surface was determined experimentally in [18]. The relevant absorption coefficients in octave bands are given in Table 1. The corresponding nominal impedance has been determined, for simplicity assumed to be real, and is also listed. Below 2 kHz, there is little variation in the measured absorption coefficient, so an average value is used for the impedance.

Table 1. Measured absorption coefficients of the tunnel surface [18] and the corresponding nominal impedance.

Frequency band (Hz)	500 Hz	1 kHz	2 kHz	4 kHz
Absorption coefficient	0.04	0.041	0.048	0.10
Normalised impedance	189.5	184.7	156.7	71.3
Nominal impedance ($\mathrm{kg \cdot s/m^2}$)	75000	75000	75000	28000

In the measurement, a loudspeaker was used as the source and the sound pressure was measured at horizontal distances of 1 m, 2 m, 5 m, 10 m, 20 m, 30 m, 40 m, 50 m and 60 m from the source. The source and the receiver were both located at 2 m above the ground in the tunnel

centre. The SPL measured at the various source-to-receiver distances relative to the level at 1 m distance was obtained in octave frequency bands from 500 Hz to 4 kHz [18].

A corresponding 2.5D acoustic FE model is created, as shown in Figure 2. The tunnel cross-section is meshed with linear quadrilateral elements, the size of which is chosen to ensure at least six elements per wavelength at 5 kHz. The source is represented by a compact source in the 2.5D model with unit volume velocity. As in the measurements, the source is located at 2 m above the ground. In the measurements, the microphones were set at the same height as the source but at different cross-sections. In the 2.5D model, however, the receiver could not be located at exactly the same cross-sectional position, so four receivers are created around the source, shifted ± 10 cm away from it in either the *y* or the *z* direction, as shown in Figure 2. Compared with the receiver-to-source distance along the tunnel direction in the measurements, the small shift will not affect the accuracy.

For comparison with the measured sound reduction in ref. [18], the SPL in the tunnel is also predicted in octave frequency bands from 500 Hz to 4 kHz. In each octave band the results are calculated at 40 frequencies spaced logarithmically between its lower and upper band limits, and the SPL is obtained by averaging the squared pressure over these 40 frequencies. The number of frequencies in each octave band is sufficient to ensure converged predictions. To obtain sound attenuation in the tunnel, the SPL is predicted at horizontal distances from 1 m to 60 m from the source with a spacing of 0.5 m. At each distance the SPL is also averaged over the four receivers, and finally normalised by the results at 1 m. The SPL in each octave band at location *x* is thus calculated as

$$L_p(x) = 10 \log_{10} \left(\frac{\langle \overline{p^2_{\mathrm{rms}}}(x) \rangle_f}{p^2_{\mathrm{ref}}} \right) \tag{23}$$

where p^2_{rms} is the mean square sound pressure in the tunnel in the spatial domain obtained from the 2.5D acoustic FE models. The overbar indicates the spatial average over the four receivers and $\langle \cdot \rangle_f$ means the average over the 40 frequencies in each band. p^2_{ref} is the mean square sound pressure at 1 m away from the source in the tunnel axis direction used as reference.

The predictions and measurements are compared in Figure 3. Generally good agreement is found, although there are some differences in the region less than 10 m from the source. The fluctuations are caused by interaction between the direct sound and the multiple reflections

from the tunnel walls. Increasing the number offrequencies in each band will tend to give smoother results but the sound attenuation remains nearly unchanged. These results based on 40 frequencies in a band are smoother than if 20 are used, but increasing further to 80 frequencies was found to give a similar level of fluctuation. Similar fluctuations are seen in measurements in a corridor by Redmore and Flockton [34]. In the 500 Hz, 1 kHz, 2 kHz bands, the SPL decays by about 12 dB in the 60 m region because of the similar absorption coefficients (≈0.04) while in the 4 kHz band, it decays by about 18 dB (the absorption coefficient is 0.10). The air absorption can also be included in the model by adding an absorption term in the axial propagation wavenumber k_x according to [17], but it is found that at 60 m from the source, the air absorption has nearly negligible effect at 500 Hz and only about 0.8 dB effect at 4 kHz.

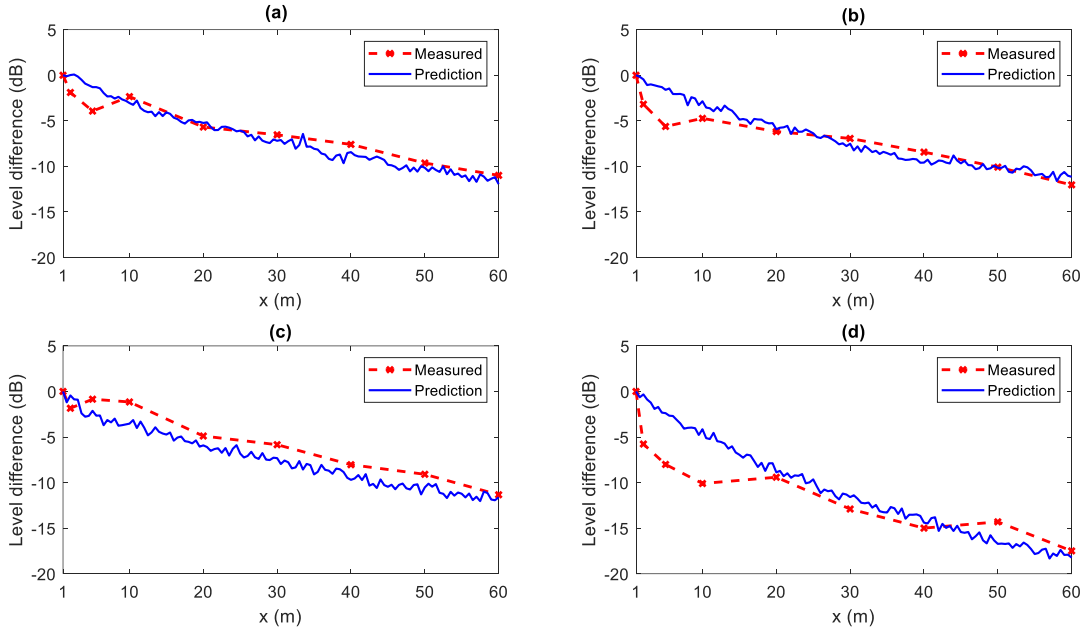

Figure 3. Octave band sound attenuation predicted by the 2.5D acoustic FE model and compared with measurements for circular railway tunnel from [18]. (a) 500 Hz, (b) 1 kHz, (c) 2 kHz, (d) 4 kHz.

3.2. Application to train exterior acoustic calculation

In this Section the 2.5D acoustic FE method is used to predict the sound distribution on the external surfaces of a train model in open field. Comparisons are made with laboratory measurements on a 1:5 scale train model performed in an anechoic chamber, as shown in Figure 4. The train model is 2.5 m long, 0.56 m wide and has a height of 0.45 m. This was mounted above a ballasted track model with the top of the sleepers 0.19 m below the train floor. A horn

driver unit driven by white noise was connected to a tube with an orifice, giving a broadly non-directional output, which represents a monopole source below the vehicle. It can be assumed that its volume velocity is independent of the source location. More details of the experimental set up can be found in ref. [21].

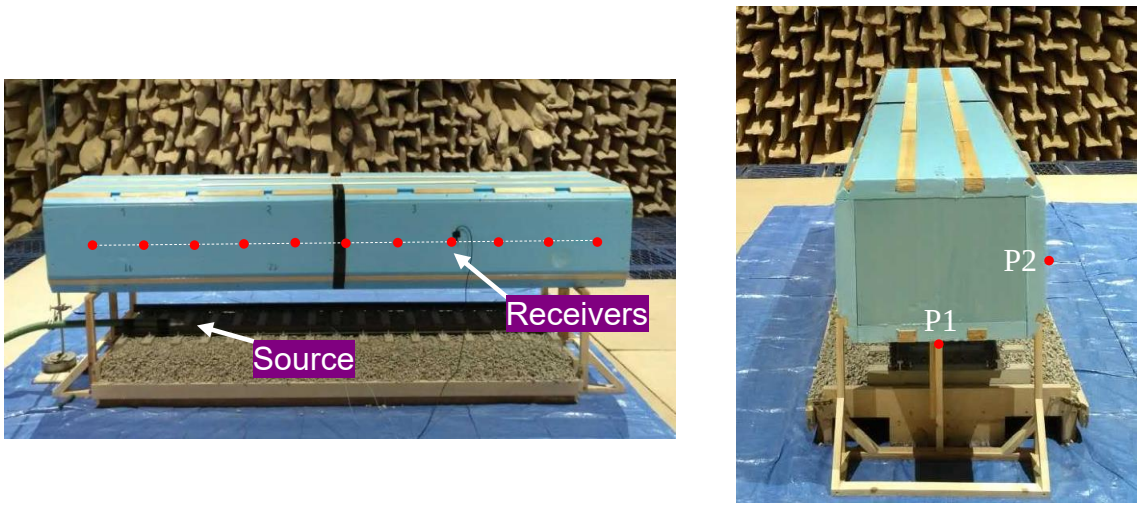

(a) (b)

Figure 4. Laboratory measurement of noise on train sides. (a) Front view, (b) side view.

A corresponding 2.5D acoustic FE model is created, as shown in Figure 5. The cross-section of the train is consistent with the measurements. The semi-circular acoustic domain around it has a radius of 2 m and meshed with linear triangular elements. The PML has a thickness of 1.5 m and meshed with linear quadrilateral elements. The other parameters of the PML are set according to ref. [23]. The ballast box in the measurement is modelled as a rectangular box with impedance boundary condition on its top. The ground on either side is assumed rigid. The size of the elements is chosen to ensure at least six elements per wavelength up to 4 kHz.

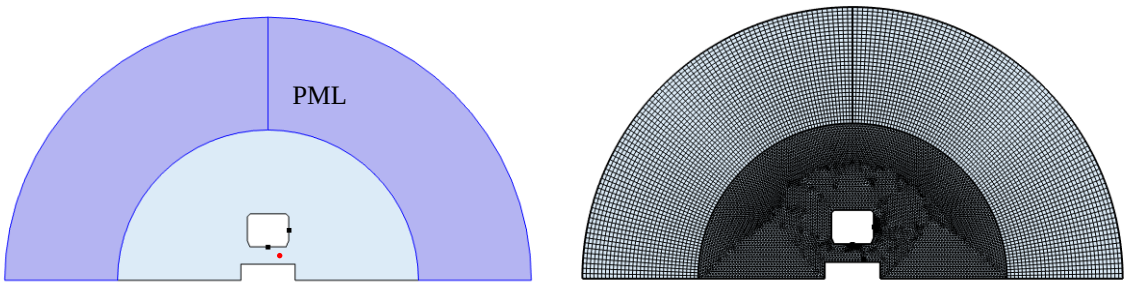

(a) (b)

Figure 5. 2.5D acoustic FE model for prediction of noise on train sides. (a) Geometry of the model, the red circle (•): source; black squares (▪): receivers, (b) mesh of the model.

The strength of the source used in the experiment was determined by a free-field measurement in the anechoic chamber. Microphones were then located along the centrelines of the bottom and right-hand side surfaces of the train in the measurements. The measured SPLs on these two surfaces of the train are compared with the results of the 2.5D FE model. The sets of receivers are marked as P1 and P2, as indicated in Figure 4(b). Predictions from the 2.5D BE method [21] are also shown here for comparison. The results from both the 2.5D models are calculated at three frequencies in each one-third octave band and averaged to obtain the SPL in these bands.

Figure 6 shows examples of the SPLs on the right-hand side surface of the train obtained from the predictions and the measurements and Figure 7 shows the corresponding results on the train bottom surface. The levels on the sides are generally around 10 dB lower than those on the bottom. It can be concluded that the agreement between the 2.5D acoustic FE model and the measurements is reasonable. The 2.5D BE and FE methods in general give similar quality of predictions although there are some differences between them (the main differences between the two 2.5D models at some locations are believed to be due to the averaging of results from slightly different sets of frequencies).

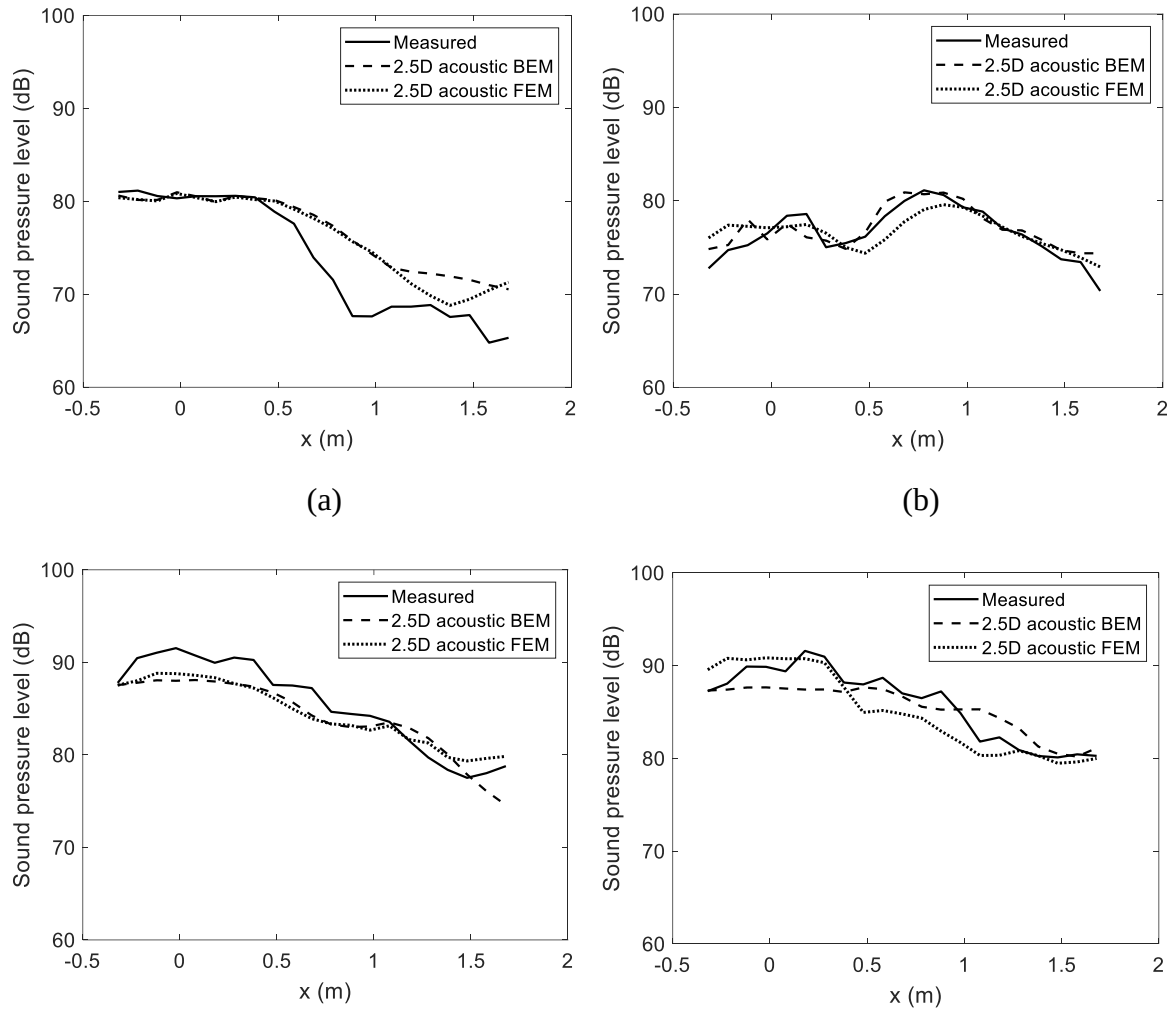

(a) (b)

(c) (d)

Figure 6. Sound distribution at the right-hand side, comparison between predictions obtained from the 2.5D acoustic FE model and the 2.5D BE model [21] with the measurements. SPL in one-third octave bands, dB re 2×10^{-5} Pa. The source is located at $x = 0$. (a) 1 kHz, (b) 1.6 kHz, (c) 2.5 kHz, (d) 4 kHz.

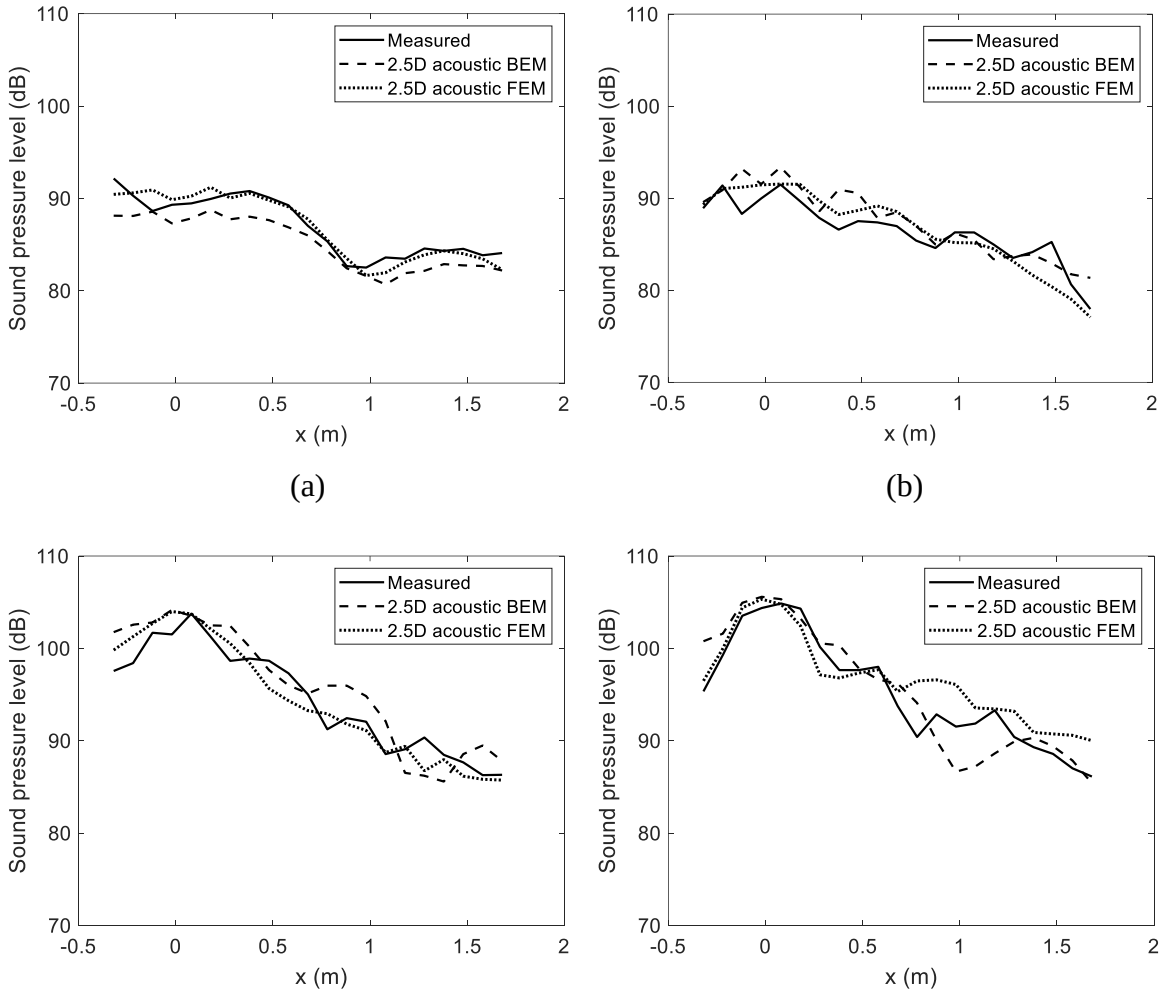

Figure 7. Sound distribution on the bottom, comparison between predictions obtained from the 2.5D acoustic FE model and the 2.5D BE model [21] with the measurements. SPL in one-third octave bands, dB re 2×10^{-5} Pa. The source is located at $x = 0$. (a) 1 kHz, (b) 1.6 kHz, (c) 2.5 kHz, (d) 4 kHz.

4. Comparison of train exterior noise in the open and in a tunnel

4.1 2.5D acoustic FE train models

Field measurements were reported in ref. [35] on a metro train in Madrid, Spain of the sound pressure distribution on the sides of a train in open field when an omnidirectional loudspeaker was located beneath the train floor. Five microphone positions were located on the train side surface directly above the loudspeaker. The height of the first position was 0.1 m above the

bottom edge of the sidewall, and the relative vertical separation between microphone positions was 0.5 m.

This case is employed here for comparison with the 2.5D acoustic FE model and is then used to investigate the difference between the sound distribution on the train external surfaces in the open and in a tunnel. Two separate models are generated. First, a 2.5D acoustic FE model with PML is created to predict the sound distribution on the train sides in the open field, as shown in Figure 8(a). The geometry of the train profile in the numerical model corresponds to the train in the tests but the details of the train floor are simplified in the model. The bogie is also omitted. A semi-circular acoustic domain with radius 5 m is created enclosing the train and meshed with linear triangular elements. The PML has a thickness of 1.5 m and meshed with linear quadrilateral elements. A monopole source is introduced in the numerical model at same location relative to the train as in the field test. The ground below the vehicle is considered as ballast, with a width of 3 m, slightly greater than the train width, 2.8 m. The surface normal impedance of the ballast is again calculated based on the Delany-Bazley model [36] with an equivalent flow resistivity of 50 $\mathrm{kPa \cdot s/m^2}$ [37]. For simplicity, outside this ballast region the surface is set to be rigid. In the second model, the same vehicle is enclosed in a tunnel, as shown in Figure 8(b). The cross-section of the tunnel from ref. [18] is adopted along with the measured absorption in that tunnel (using the nominal impedance as in Section 3). The ground in the tunnel is considered as rigid for a slab track and as absorptive for a ballasted tack. In both models the minimum element size is about 2 cm in order to have at least six elements in each wavelength at 2 kHz.

Five receivers are considered on the side of the train, 2 cm from the train surface, representing the five microphones in the measurements. A further three receivers are considered at the centre of the other three surfaces, as shown in Figure 8.

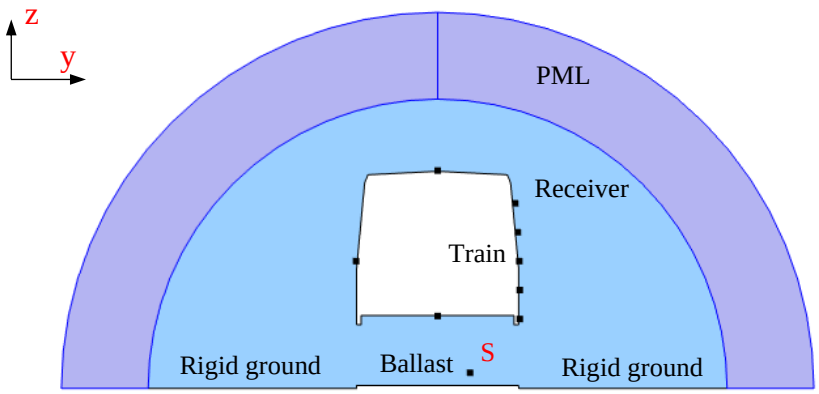

(a)

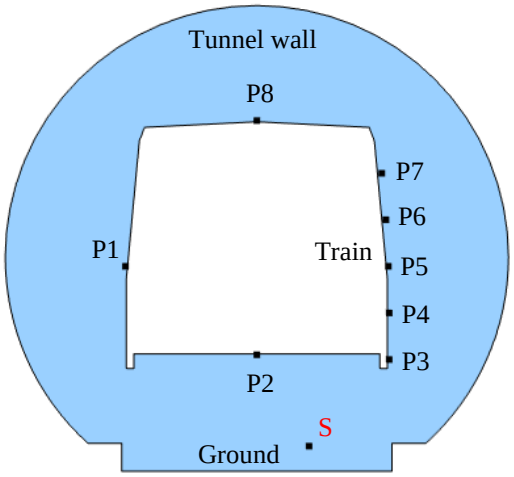

(b)

Figure 8. 2.5D acoustic FE model for noise on the exterior of a train due to a monopole source. (a) In open field, (b) in a tunnel.

4.2 Sound spatial distribution on the train external surface

In Figure 9, the predicted SPL along the vertical line on the train external surface in the open is compared with the measurements. As the source strength of the loudspeaker used in the field test is not available, the volume velocity is set in the predictions to ensure that the average predicted SPLs correspond roughly to the measured ones for ease of comparison. The distribution of sound pressure level is presented in one-third octave bands (averaged over three frequencies in each one-third octave band for the prediction) for four example frequency bands. It can be seen that the 2.5D FE model captures the trend of the sound pressure distribution, decreasing with increasing height on the side surfaces, and the predictions match the

measurements well. The predictions from ref. [21] obtained from the 2.5D BE model are also included for comparison. The two different models give similar results, although there are some differences in the 1600 Hz band which are believed to be due to slight differences in the cross-section of the train in the two models.

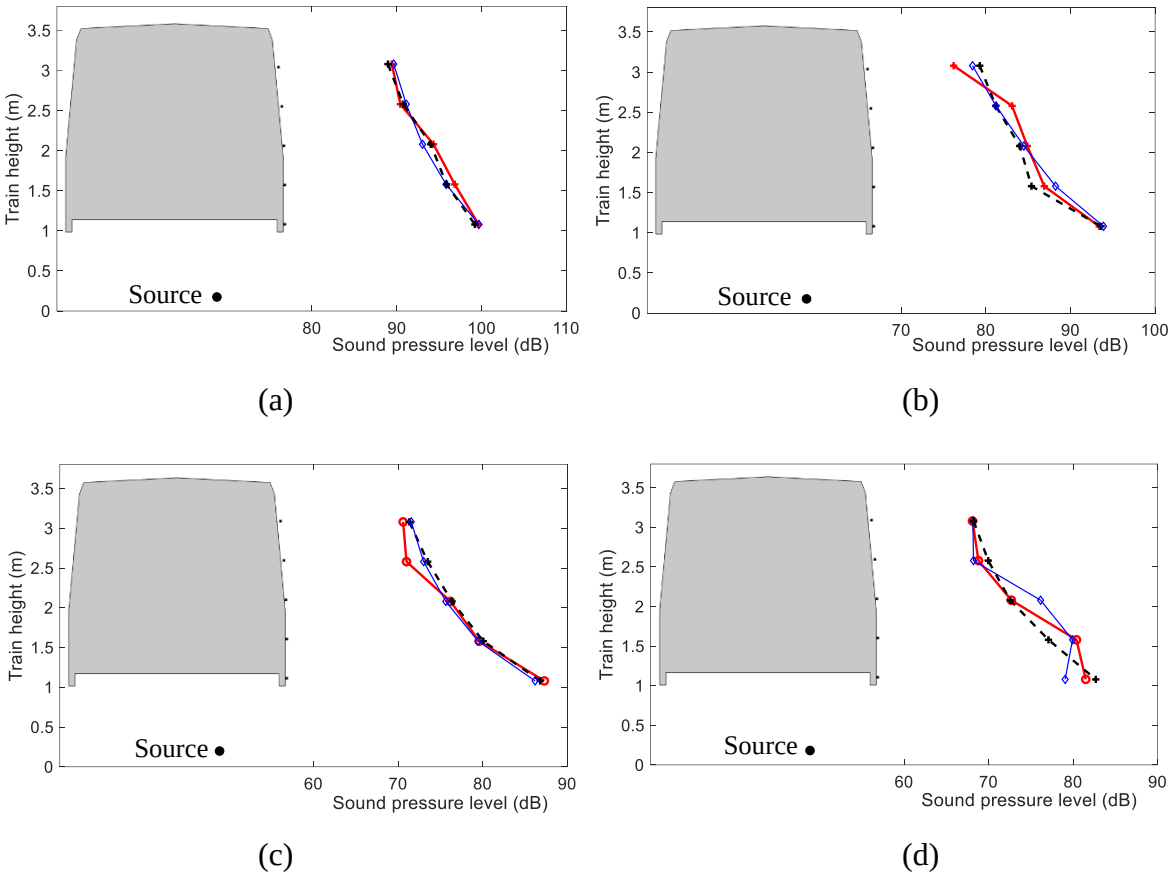

Figure 9. Sound distribution with train height obtained from measurement [35] and from the 2.5D acoustic models in one-third octave bands, dB re 2×10^{-5} Pa. —○—: Measured [21]; —◇—: 2.5D BE model [21]; - + -: 2.5D acoustic FE model. (a) 200 Hz, (b) 400 Hz, (c) 800 Hz, (d) 1.6 kHz.

The SPLs calculated using the 2.5D acoustic FE model at these positions on the train external surface are compared in Figure 10 between the open field and the tunnels with slab track and ballasted track. In the tunnel cases, there are greater variations between different frequencies, so 20 frequencies are used in each one-third octave band (sufficient for converged solutions). The same source strength as above is used in each case. The results are shown for the same four frequency bands in Figure 10. In the tunnel with the ballasted track, the SPL on the train

sides (close to the source) is increased by about 10 dB on average compared with the values in open field. If the tunnel is built with slab track, there is a further 6 dB increase on average.

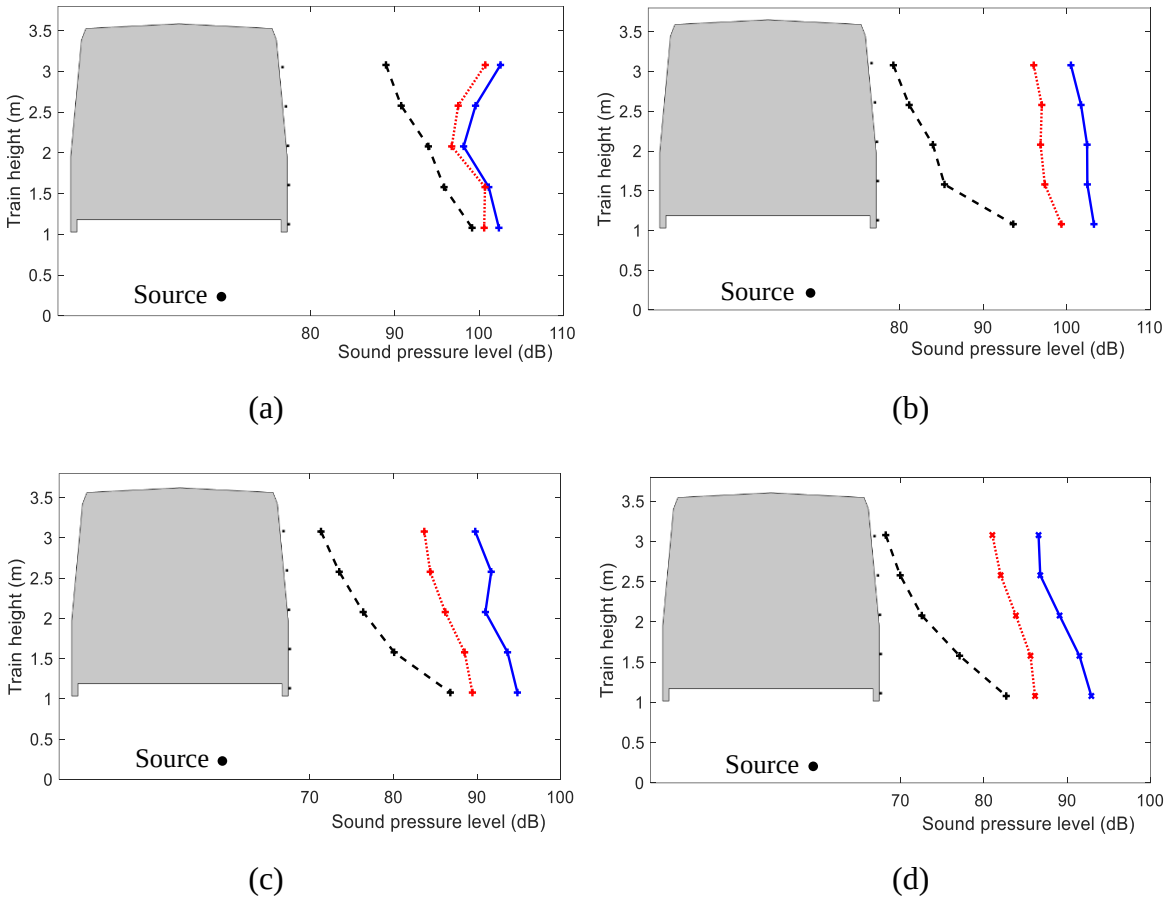

Figure 10. Sound distribution with train height in one-third octave bands due to a monopole source, dB re 2×10^{-5} Pa. - + -: in the open field; —+—: in the tunnel with slab track; ···+···: in the tunnel with ballasted track. (a) 200 Hz, (b) 400 Hz, (c) 800 Hz, (d) 1.6 kHz.

Figure 11 shows the sound level distribution along the train on its four surfaces in the 1.6 kHz band as an example (receivers marked as P1, P2, P5, P8 in Figure 8). In the open field, Figure 11(a), there are large differences between the SPL on the four surfaces: the bottom has the highest level as there is direct sound, followed by the right-hand side surface, which is about 15 dB lower. The SPL on the left-hand side of the train is slightly lower than that on the right because it is further from the source. The SPL on the roof is about 40 dB lower than on the bottom and 15 dB lower than on the sides. At 20 m from the source, the SPL is reduced by 25 dB on the bottom, and about 12 dB on the sides, whereas on the top surface there is nearly no decay.

The results for tunnels with slab track and ballasted track show similar trends. The SPL is much higher in these cases and reduces with distance at a lower rate. The SPLs on the sides and roof are similar to each other.

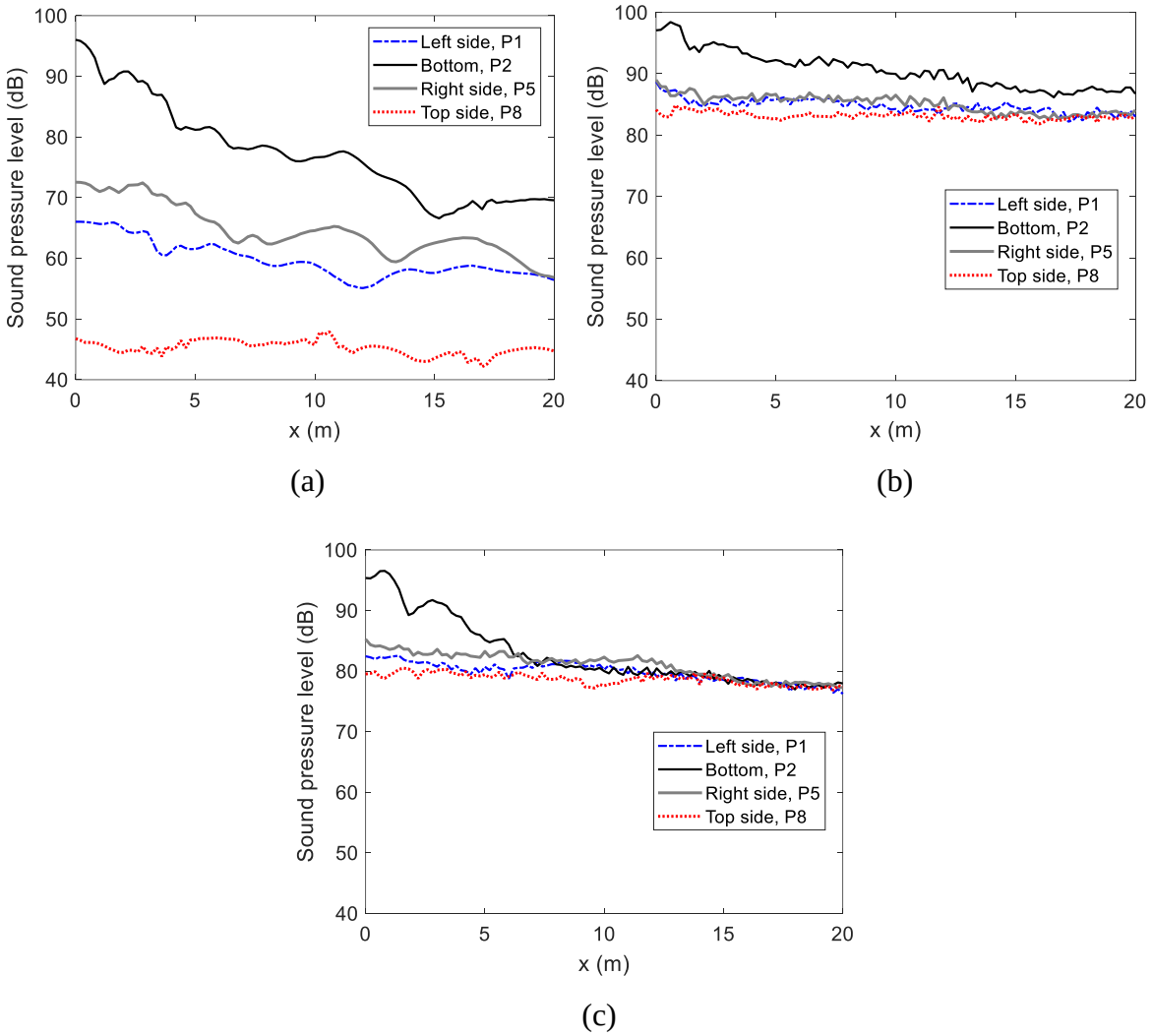

Figure 11. Sound distribution along the train in the 1.6 kHz one-third octave band due to a monopole source under the train, dB re 2×10^{-5} Pa. (a) In the open field, (b) in the tunnel with slab track, (c) in the tunnel with ballasted track.

Figure 12 shows the sound level distribution on the train cross-section in the form of an equivalent polar plot for the 800 Hz band as an example. This section is in the same plane as the source. When the train is in open field, the sound pressure on the train floor is much higher than on the sides and the SPL on the roof is about 40 dB lower than that on the train floor. In the tunnels, the SPLs on the train floor are similar to the values in the open field but the SPLs on the train side and roof surfaces increase significantly and become more evenly distributed. The SPL on the right-hand side surface increases by about 10 dB (on average) and the values

on the roof increase by about 30 dB when it is in the tunnel with a ballasted track. In the tunnel with a slab track, the SPLs on the train side and roof surfaces increase by about a further 6 dB.

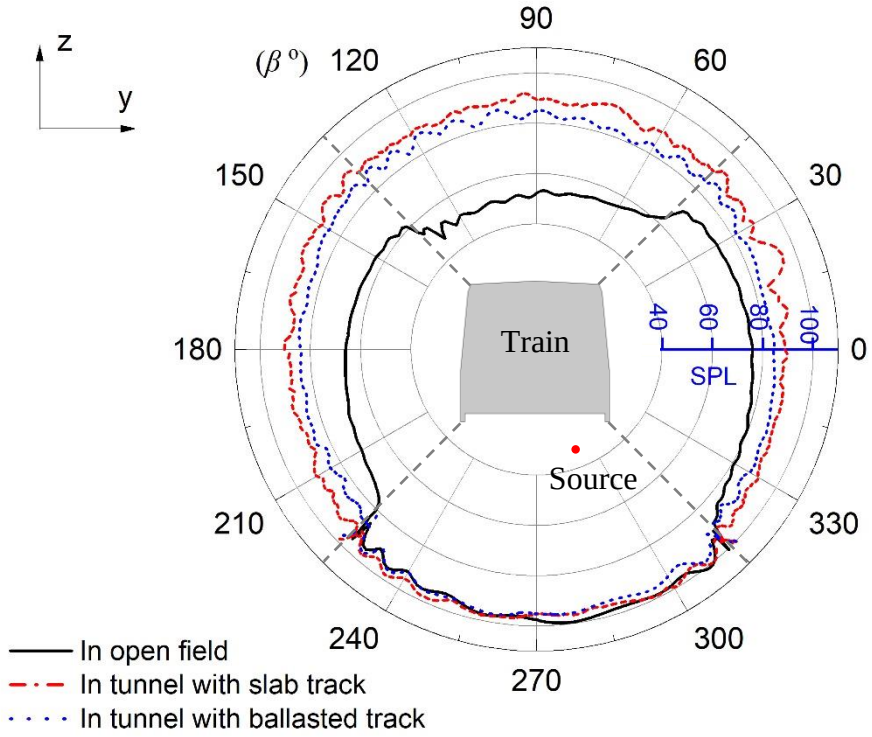

Figure 12. Sound distribution on the train external surfaces (the same cross-section as the source) in the 800 Hz one-third octave band due to a monopole source, dB re 2×10^{-5} Pa.

4.3 Sound spectrum on the train external surface

Figure 13 shows the frequency spectra of sound pressure on the train side at receiver P5 for the three cases. The sound pressure is calculated with a frequency resolution of 1 Hz and normalised by the source strength. In the three cases, the normalised sound pressure increases with increasing frequency, but fluctuations appear. In the open field, diffracted sound waves, including reflections from the ground, interact on the train side surface, which causes some fluctuations in the sound spectrum. In the tunnels, however, acoustic modes exist, and many peaks can be found in the sound spectrum. Due to the presence of the tunnel surfaces, the sound pressure increases compared to the open field.

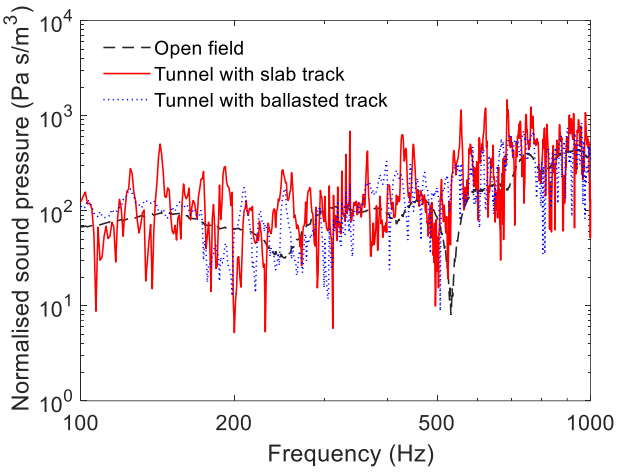

Figure 13. Sound pressure on the train side surface at receiver P5 normalised by volume velocity.

Figure 14 shows the one-third octave frequency spectra of SPL on the centreline of each surface at x=0 m for the three cases: in the open, and in the tunnels with slab and ballasted track. These results are calculated using 20 frequencies in each one-third octave band which has been found to be sufficient to achieve convergence. The results on the four surfaces in the open show great differences in SPL, whereas in the tunnels, the SPL spectra on the two sides and the top are similar and that on the bottom is about 10 dB higher. Compared with the result in the open, above 250 Hz the SPL on the train side in the tunnels increases by a nearly constant amount of about 10 dB for the tunnel with ballasted track and 16 dB for the one with slab track.

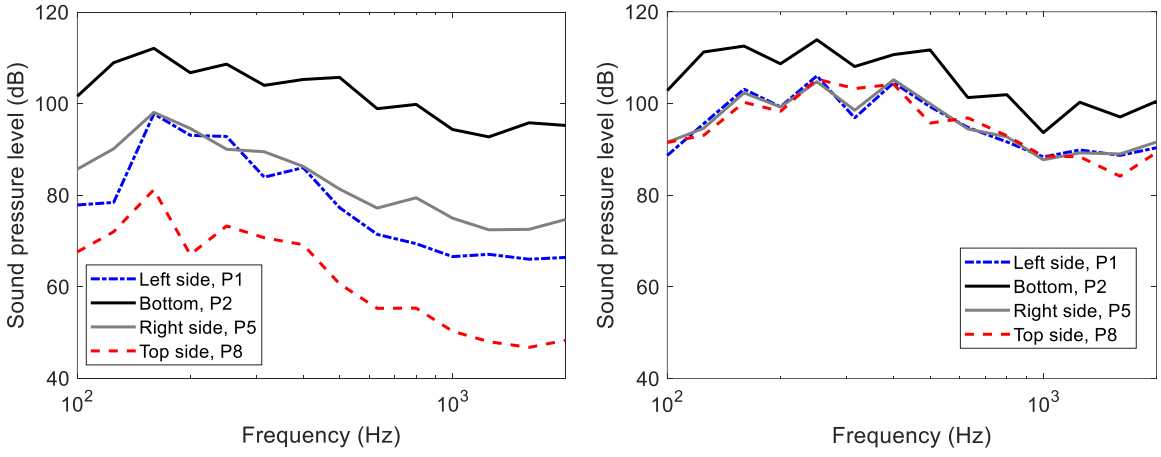

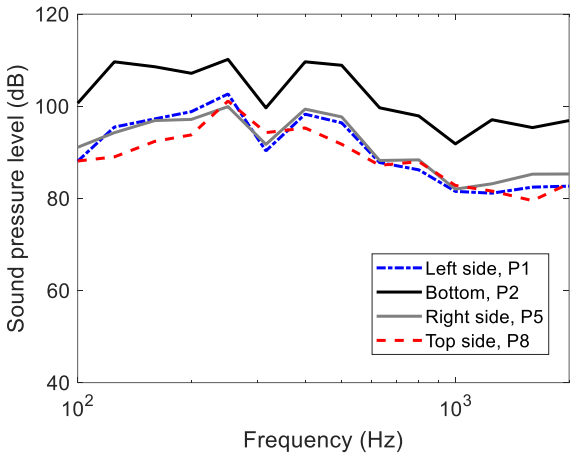

(c)

Figure 14. SPL on the centreline of each surface at x=0 m, in one-third octave frequency bands due to a monopole source beneath the train. (a) In the open field, (b) in the tunnel with slab track, (c) in the tunnel with ballasted track, dB re 2×10^{-5} Pa.

5. Discussion

Compared with the 2.5D BE method [5], the 2.5D acoustic FE method presented here can more easily model sources within the acoustic domain. In the 2.5D models, the results are calculated as a spectrum of wavenumber. To use the 2.5D BE model, the system matrices are wavenumber dependent and need to be recalculated at every wavenumber. To use the 2.5D FE model, the system matrices are independent of the wavenumber, and therefore they can be assembled once and be used for all wavenumbers. Despite the need to include a larger number of elements, therefore, the 2.5D FE models can be more efficient than the 2.5D BE models. If the same mesh is used for all frequencies, the relative efficiency of the two models will be frequency independent.

In common with any other 2.5D model, the 2.5D acoustic FE model can be used for problems that have a constant cross-section and are extended infinitely in one direction. If the object has a restricted length in the direction in which the Fourier transform is applied, this will have some effects on the accuracy. Besides, the method cannot model discontinuities in the axial direction. For example, it is less suitable for predicting the sound pressure incident on the train floor than the train sides because the equipment mounted beneath the train floor causes scattering of sound below the vehicle. Besides, the gaps between two adjacent carriages cannot be included in the model.

6. Conclusions

A 2.5D FE method is presented to study acoustic problems that have uniform properties in one direction, which are common in the railway field. Boundary conditions based on prescribed normal velocity or acoustic impedance are implemented as well as internal acoustic sources. To allow for a free field, a perfectly matched layer is added in the 2.5D domain.

The model has been applied to the sound attenuation in tunnels and is found to agree well with published measurements. Predictions of the sound incident on the sides of a train in the open due to a source below the train also show good agreement with measurements. The above comparisons have shown that the 2.5D acoustic FE method has wide application and can give good quality predictions of noise for both interior and exterior acoustic problems.

Finally, the effect of a tunnel on the sound distribution on the external surfaces of a metro vehicle has been studied using the model. The predictions show that in a tunnel with ballasted track, the sound pressure levels on the train sides in the region close to the source increase by about 10 dB on average above 250 Hz compared with the open field case. If the tunnel is built with slab track, there is a further 6 dB increase on average, similar to experimental results found in the literature [2, 3]. The increase of the sound pressure level on the top surface of the train is even greater, with similar levels to the train sides. The above analysis can be used further to investigate the effect on the interior noise of railway vehicles when they are running in tunnels.

References

[1]. J. Zhang, X. Xiao, X. Sheng, D. Yao, R. Wang, An acoustic design procedure for controlling interior noise of high-speed trains, Applied Acoustics 168 (2020) 107419.

[2]. M. Heckl, G. Hauck, R. Wettschureck, Structure-borne sound and vibration from rail traffic, Journal of Sound and Vibration 193(1) (1996) 175-184.

[3]. S. Choi, C.W. Lee, J.C. Kim, J.H. Cho, Interior noise of a korean high-speed train in tunnels. Proceedings of ACOUSTICS 2004, Gold Coast, Australia, 2004.

[4]. J. Han, X. Xiao, Y. Wu, Z. Wen, G. Zhao, Effect of rail corrugation on metro interior noise and its control, Applied Acoustics 130 (2018) 63-70.

[5]. D. Duhamel, Efficient calculation of the three-dimensional sound pressure field around a noise barrier, Journal of Sound and Vibration 197(5) (1996) 547-571.

[6]. D. Thompson, Railway noise and vibration: mechanisms, modelling and means of control, Elsevier, Oxford, 2008.

[7]. B.K. Kim, J.G. Ih, On the reconstruction of the vibro-acoustic field over the surface enclosing an interior space using the boundary element method, The Journal of the Acoustical Society of America 100(5) (1996) 3003-3016.
[8]. R.H. Lyon, R.G. DeJong, eds. Theory and application of statistical energy analysis, Butterworth-Heinemann, 1995.
[9]. J. Forssén, S. Tober, A.C. Corakci, A. Frid, W. Kropp, Modelling the interior sound field of a railway vehicle using statistical energy analysis, Applied Acoustics 73(4) (2012) 307-311.
[10]. M. Sadri, J. Brunskog, D. Younesian, Application of a Bayesian algorithm for the Statistical Energy model updating of a railway coach, Applied Acoustics 112 (2016) 84-107.
[11]. F. Fahy, A note on the subdivision of a volume of air in a vehicle enclosure into sea subsystems, Journal of Sound Vibration 271 (2004) 1170-1174.
[12]. H. Jang, C. Hopkins, Prediction of sound transmission in long spaces using ray tracing and experimental Statistical Energy Analysis, Applied Acoustics 130 (2018) 15-33.
[13]. T. Kohrs, K.R. Kirchner, D. Fast, Sound propagation and distribution around typical train carbody structures, in InConference Proceedings, Euronoise. 2018.
[14]. A.D. Pierce, Acoustics: An introduction to its physical principles and applications, Acoustical Society of America, 1990.
[15]. D. Blokhintzev, The propagation of sound in an inhomogeneous and moving medium I. The Journal of the Acoustical Society of America 18(2) (1946) 322-328.
[16]. A. Bistagnino, A. Vallespín, J. Sapena, Prediction of Acoustical Wall Pressure Levels of Rolling Stock Vehicles, Notes on Numerical Fluid Mechanics & Multidisciplinary Design 126 (2015) 675-682.
[17]. K.M. Li, K.K. Iu, Full-scale measurements for noise transmission in tunnels, The Journal of the Acoustical Society of America 117(3) (2005)1138-1145.
[18]. W.S.W. Fung, A study on transmission of noise in railway tunnel, PhD thesis, the Hong Kong Polytechnic University, China, 2010.
[19]. D.Hothersall, S. Chandler-Wilde, M. Hajmirzae, Efficiency of single noise barriers, Journal of Sound and Vibration, 146(2) (1991) 303-322.
[20]. X. Zhang, G. Squicciarini, D.J. Thompson, Sound radiation of a railway rail in close proximity to the ground, Journal of Sound and Vibration. 362 (2016) 111-124.
[21]. H. Li, D. Thompson, G. Squicirrini, X. Liu, M. Rissmann, F. D. Denia, J. Giner-Navarro, Using a 2.5D boundary element method to predict the noise on the train side due to rolling noise, Journal of Sound and Vibration 486 (2020) 115599.
[22]. Y. Lam, A boundary integral formulation for the prediction of acoustic scattering from periodic structures, The Journal of the Acoustical Society of America 105(2) (1999) 762-769.
[23]. Fard, S.M.B, Peters, H., Kessissoglou, N. and Marburg, S., Three-dimensional analysis of a noise barrier using a quasi-periodic boundary element method. The Journal of the Acoustical Society of America 137 (2015) 3107-3114.
[24]. Ziegelwanger, H., Reiter, P. and Conter M., The three-dimensional quasi-periodic boundary element method: implementation, evaluation, and use cases. International Journal of Computational Methods and Experimental Measurements 5 (2017) 404-414.
[25]. M. Karimi, P. Croaker, N. Kessissoglou, Boundary element solution for periodic acoustic problems, Journal of Sound and Vibration 360 (2016) 129-139.
[26]. Mace, B.R., Duhamel, D., Brennan, M.J. and Hinke, L., Finite element prediction of wave motion in structural waveguides. The Journal of the Acoustical Society of America 117 (2005) 2835-2843.

[27]. C.M. Nilsson, S. Finnveden, Waves in thin-walled fluid-filled ducts with arbitrary cross-sections, Journal of Sound and Vibration 310(1-2) (2008) 58-76.
[28]. F.Q. Hu, On absorbing boundary conditions for linearized Euler equations by a perfectly matched layer, Journal of Computational Physics 129(1) (1996) 201-219.
[29]. P. Zuo, Z. Fan, SAFE-PML approach for modal study of waveguides with arbitrary cross sections immersed in inviscid fluid, Journal of Sound and Vibration 406 (2017) 181-196.
[30]. W. Duan, R. Kirby, Guided wave propagation in buried and immersed fluid-filled pipes: Application of the semi analytic finite element method, Computers & Structures 212 (2019) 236-247.
[31]. X. Song, Q. Li, D. Wu, Investigation of rail noise and bridge noise using a combined 3D dynamic model and 2.5 D acoustic model, Applied Acoustics 109 (2016) 5-17.
[32]. L.Y. Tio, A.A. Gibson, B.M. Dillon, L.E. Davis, Weak form finite element formulation for the Helmholtz equation, International Journal of Electrical Engineering Education 41(1) (2004) 1-9.
[33]. M. Petyt, Introduction to finite element vibration analysis, Cambridge university press, 2010.
[34]. T. Redmore, S. Flockton, A design formula for predicting the attenuation of sound along a long corridor, Acoust Lett. 1 (1977) 21-24.
[35]. H. Li, D. Thompson, G. Squicciarini, X. Liu, M. Rissmann, F.D. Denia, J. Giner-Navarro, L. Baeza, J. Moreno, J. M. Jarillo, A framework to predict the noise inside railway vehicles with application to rolling noise, Applied Acoustics 179 (2021) 108064.
[36]. M. Delany, E. Bazley, Acoustical properties of fibrous absorbent materials, Applied Acoustics 3(2) (1970) 105-116.
[37]. X. Zhang, Modelling of track sound radiation, PhD thesis, the University of Southampton, UK, 2016.